



# Hybrid life-extending control of mechanical systems: experimental validation of the concept<sup>☆</sup>

Hui Zhang<sup>a</sup>, Asok Ray<sup>a,\*</sup>, Shashi Phoha<sup>b</sup>

<sup>a</sup>Mechanical Engineering Department, The Pennsylvania State University, 137 Reber Building, University Park, PA 16802, USA

<sup>b</sup>Information Systems Division, Applied Research Laboratory, The Pennsylvania State University, University Park, PA 16802, USA

Received 7 September 1998; revised 6 January 1999; received in final form 12 April 1999

*Structural durability and high performance of mechanical systems can be achieved by two-tier hybrid life extending decision and control. Experimental results on a laboratory test apparatus are presented for validation of the proposed concept.*

---

## Abstract

The goal of life-extending control is to achieve high performance of complex dynamical systems (e.g., aircraft, spacecraft, and energy-conversion systems) without overstraining the mechanical structures and the potential benefit is an increase in the service life of critical components with no significant loss of performance. This paper presents a two-tier architecture and a design methodology of hybrid (i.e., combined discrete-event and continuously varying) life-extending control for structural durability and high performance of mechanical systems. A feedback controller at the lower tier is designed with due consideration to robust performance and damage mitigation. A variable-structure stochastic automaton is employed at the lower tier for status evaluation of structural damage while the overall system performance is maintained by the supervisory level discrete-event controller at the upper tier. Experimental results on a laboratory test apparatus are presented for validation of the proposed concept of hybrid life-extending control. © 1999 Elsevier Science Ltd. All rights reserved.

*Keywords:* Hybrid control; Life extending control; Robust control; Supervisory control

---

## 1. Introduction

A major goal in the control of dynamical systems such as advanced aircraft, spacecraft, and energy-conversion systems is to achieve high performance with enhanced reliability, availability, component durability, and maintainability. The concept of life-extending control, also referred to as damage-mitigating control, is built upon

the hypothesis that substantial improvement in the service life of critical plant components can be achieved with no significant loss of the system dynamic performance. Life-extending control of mechanical systems is a relatively new area of research that combines the two distinct disciplines: *Systems Sciences and Mechanics of Materials*. Currently, there is a rather limited amount of information available on this topic in open literature. Ray, Wu, Carpino and Lorenzo (1994) and Dai and Ray (1996) have shown that, in an open-loop setting, it is feasible to reduce the damage increment and accumulation in critical plant components without any appreciable loss of plant performance. Subsequently, synthesis of life-extending control systems has been reported by Kallappa, Holmes and Ray (1997), Holmes and Ray (1998), and Rozak and Ray (1997, 1998) for different applications including fossil power plants, rocket engines, and rotorcraft in the setting of continuously varying feedforward and feedback systems. Ray and Weng (1995) have proposed the architecture of a

---

<sup>☆</sup>The work reported in this paper was supported in part by: National Science Foundation under Research Grant Nos. DMI-9424587 and CMS-9531835; NASA Langley Research Center under Grant No. NCC-1-249; National Academy of Sciences under a Research Fellowship Award to the second author. This paper was not presented at any IFAC meeting. This paper was recommended for publication in revised form by Associate Editor M. Tomizuka under the direction of Editor K. Furuta.

\*Corresponding author. Tel.: + 1-814-865-6377; fax: + 1-814-863-4848.

E-mail address: axr2@psu.edu (A. Ray)

hierarchically structured hybrid (i.e., combined continuously varying and discrete event) decision and control system that integrates life-extending control with planning and scheduling of plant maintenance and operation.

Realization of the life-extending control concept may require augmentation of systems-theoretic and approximate reasoning techniques (Holmes & Ray, 1998) for synthesis of decision and control laws with governing equations and inequality constraints that represent the mechanical behavior of structural materials for the purpose of damage representation and life prediction. The major challenge here is to characterize the damage generation process and then utilize this information for synthesizing algorithms of robust control, diagnostics, and risk prediction in complex mechanical systems.

This paper introduces the concept of hybrid (i.e., combined discrete-event and continuously-varying) life-extending control for structural durability and high performance of mechanical systems, and proposes a two-tier architecture and a methodology for controller design. Experimental results are presented for validation of the hybrid life extending control concept on a special-purpose test apparatus (Zhang & Ray, 1999). Case studies indicate that fatigue life of test specimens can be substantially extended with no appreciable degradation in the system dynamic performance. The steps for design of the control system are delineated below:

- frequency-domain identification of the plant (e.g., test apparatus) dynamics and modeling uncertainties in the state-space setting based on experimental data (Bayard, 1992, 1993) and fundamental principles of physics;
- robust controller synthesis based on  $H_\infty$ -optimization by taking both plant-dynamic performance and structural degradation into consideration (Kallappa et al., 1997; Holmes & Ray, 1998; Rozak & Ray, 1998);
- damage status evaluation and decision-making based on variable-structure stochastic automaton (Narendra & Thathachar, 1989); and
- adjustment of plant performance reference for discrete-event supervisory control with continuous-to-discrete and discrete-to-continuous interfaces (Stiver, Antsaklis & Lemmon, 1995).

## 2. Decision and control system architecture

The concept of hybrid life-extending decision and control of mechanical structures is realized following a two-tier hierarchical architecture as shown in Fig. 1. The rationale for this hierarchical approach is to partition the

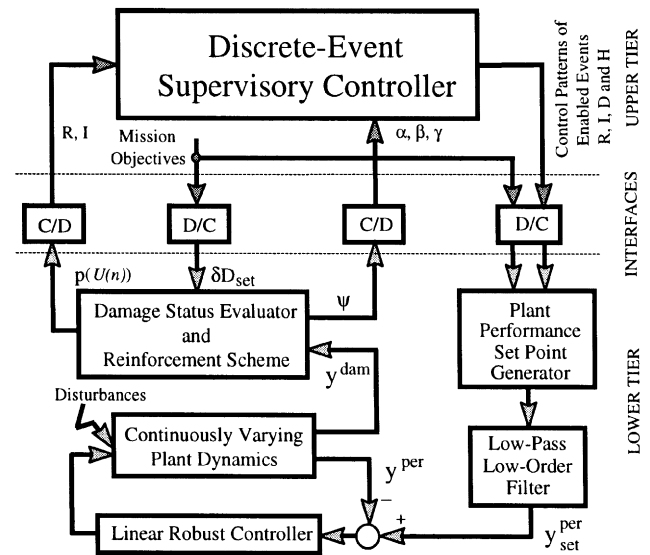


Fig. 1. Architecture of the hybrid life-extending control system.

control system into two different layers, which can operate more or less autonomously in conjunction with appropriate input/output interfaces. Tracking of dynamic performance is accomplished by the robust linear controller, at the lower tier, which is synthesized via well-known  $H_\infty$ -based techniques in the continuous setting (Kallappa et al., 1997; Holmes & Ray, 1998). The remaining functional modules in the lower tier are: (i) Plant Performance Set Point Generator and Low-pass Low-order Filter; and (ii) Damage Status Evaluator and Reinforcement Scheme. Based on the discrete-event commands issued by the supervisory controller at the upper tier, the plant performance set-point generator tunes the continuous signal as the reference trajectory for the linear closed-loop system. To prevent any abrupt changes in the physical plant, the reference signal is shaped by a low-order low-pass filter. Since the dynamics of damage in structural materials are highly nonlinear and uncertain, the life-extending control laws at the lower tier cannot be easily implemented in the deterministic setting of linear  $H_\infty$ -control. Therefore, the damage-status evaluator and the reinforcement scheme are formulated based on a nonlinear stochastic dynamic model of material degradation (Ray, 1999; Ray & Patankar, 1999) and the reward-penalty properties of a variable-structure stochastic automaton (Narendra & Thathachar, 1989), respectively. The information on material degradation, generated from the statistics of damage and damage increment, is used to identify probabilities of a finite number of actions for modification of the performance set point. When a specific action is executed, the environment provides a random response. The reinforcement scheme determines how the choice of actions at any stage is guided by the current and past

responses. The lower tier of the hybrid control system thus generates a combination of different continuously varying signals that interact, in real time, with the (discrete-event) supervisory controller at the upper tier via continuous-to-discrete (C/D) and discrete-to-continuous (D/C) interface as seen in Fig. 1.

The mission objectives that represent the desired life span and performance of the plant are also inputs to the D/C interfaces. The set points of damage increment and plant performance are generated by the D/C interfaces, based on the mission objectives and are passed to the Damage Status Evaluator and the Plant Performance Set Point Generator, respectively. Directly setting the damage increment set point  $\delta D_{\text{set}}$  may not be meaningful as the damage increment  $\delta D$  dynamically changes with respect to the elapsed life of structural component(s). For example,  $\delta D_{\text{set}}$  may be required to vary with the age of the plant even though the performance specifications may remain unchanged. The D/C interfaces must be intelligent and their design for more complex machinery is a subject of future research. A deterministic state-space model of fatigue crack damage and its extension to a stochastic model are briefly described in Appendices A and B, respectively. Details are reported by Patankar, Ray and Lakhtakia (1998), Ray (1999), and Ray and Patankar (1999).

The discrete-event supervisory controller at the upper tier makes decisions to update the reference trajectory (i.e., set point) of performance based on the following input information:

- Sensory information on plant performance and structural damage as uncontrollable events  $\alpha$ ,  $\beta$  and  $\gamma$ .
- A finite number of actions for modification of performance set point, as controllable events  $R$  and  $I$ .

The supervisory controller operates on the discrete-event plant model that is formulated based on the knowledge of the continuously varying plant and controller at the lower tier. The outputs of the supervisory controller transmit the decisions, in real time, as control patterns down to the lower tier and may also report the plant performance and damage status to an external agent. Discrete-event phenomena at the supervisory level are modeled as interacting *finite-state automata* following the recent work in this field (Ramadge & Wonham, 1987; Kumar & Garg, 1995; Garcia & Ray, 1996). In this setting, for example, the states of an automaton reflect the damage status (e.g., the material degradation with respect to the need for maintenance, repair, or part replacement) of a plant subsystem. The events interconnecting the states correspond to discrete and abrupt changes in the state of equipment health, or gradual degradation of the material condition as it crosses a

predetermined threshold of the predicted remaining life. The set of events is further partitioned into the subsets of *controllable* events and *uncontrollable* events. A controllable event is one whose occurrence can be prevented by some control action from the upper level. An example of controllable event is the action of taking a component off-line to prevent a catastrophic failure. An uncontrollable event is one that is not directly controllable from any level (e.g., exogenous disturbances to the plant and failures anywhere in the control system).

### 3. Description of the test apparatus

The test apparatus is briefly described in this section and the details of mechanical design and instrumentation are reported in a previous publication (Zhang & Ray, 1999). The test apparatus is designed and fabricated as a three-degree-of-freedom (DOF) mass-beam structure that is excited by the oscillatory motion of two vibrators as shown in Fig. 2. Two of the three DOFs are directly controlled by the two actuators (i.e., Vibrator #1 and Vibrator #2). Displacements of the three vibrating masses: Mass #1, Mass #2, and Mass #3, are directly measurable. The inputs to the multivariable mechanical structure are forces exerted by the two actuators and the output to be controlled is the displacement of Mass #1. A failure site is introduced 25.4 mm (1 in) from Mass #3 in the test specimen (Beam #2) which represents a critical plant component subjected to fatigue crack damage.

The test apparatus is logically partitioned into two subsystems: (i) the plant subsystem consisting of the mechanical structure including the test specimen to undergo fatigue damage; and (ii) the control and instrumentation subsystem consisting of actuators, and sensors, computers for data acquisition and processing and control-law execution, and data communications hardware and software. The frequency of the (square-wave) reference signal is 2.07 Hz that is one-third of the first modal frequency ( $\sim 6.21$  Hz) of the test apparatus structure. Hence, the third harmonic of the reference signal excites the structure at the resonance frequency of 6.21 Hz. Thus, the test specimen can be excited at different levels of cyclic stress via vibratory motion of Mass #3 with no significant change in the external power injection into the actuators.

The material of the test specimen is 6063-T6 aluminum alloy. The cyclic stress at the failure site is the damage-causing variable that needs to be appropriately regulated by the damage-mitigating controller for enhancement of structural durability without any significant loss of the system performance. The far-field cyclic stress at the failure site is obtained from a finite-element model of the test apparatus structure

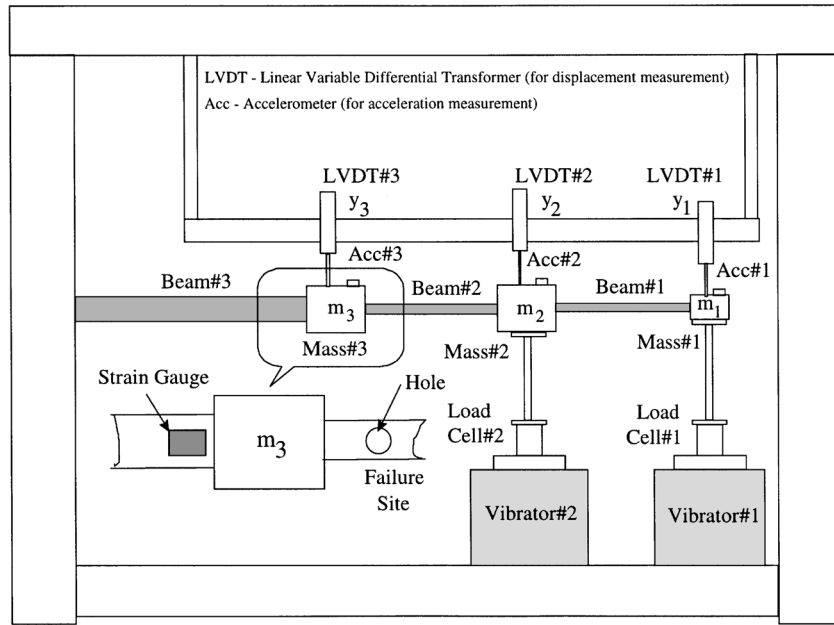


Fig. 2. Schematic diagram of the test apparatus.

and is validated with experimental data of strain measurements to be within 5% accuracy. This model generates the estimated far-field stress  $\hat{S}(t)$  in real time as an algebraic function of the displacement measurements of the three vibrating masses: Mass #1, Mass #2, and Mass #3:

$$\hat{S}(t) = \sum_{k=1}^3 \beta_k v_k(t) \quad \text{with } \beta_1 = 1.5025,$$

$$\beta_2 = -9.4095, \quad \beta_3 = 13.1437 \text{ in SI units.} \quad (1)$$

#### 4. System identification for robust control synthesis

The structure of the open-loop plant model is derived based on a priori information (e.g., fundamental laws of physics, plant operating conditions, and physical dimensions). Although the plant model parameters can be identified via either time-domain or frequency-domain techniques, we have chosen frequency-domain approach for identification of modeling uncertainties as needed for  $H_\infty$ -based synthesis of a robust control system for the resonance-dependent test apparatus under consideration. Apparently, commercially available codes (e.g., the Matlab System Identification Toolbox™ and Frequency Domain Identification Toolbox™) are inadequate for this specific application because they only generate either system-parameter estimation error or curve-fitting error. The state-space identification method, used in this research, is built

upon the *State-Space from Frequency Data (SSFD)* algorithm of Bayard (1993). The identification procedure starts from construction of an excitation signal that is a Schroeder-phased multi-sinusoidal input. This signal is applied to each input (i.e., actuator) of the plant, one at a time, until the respective output reaches the steady state. The steady-state input/output data are acquired and then averaged via spectral estimation processing. Subsequently, a complete multiple-input multiple-output (MIMO) plant estimate is constructed from the series of single-input multiple-output (SIMO) experiments. The plant spectral estimate is then curve-fitted by minimizing a weighted Euclidean-norm error criterion to obtain a multivariable transfer matrix in the polynomial form.

The transfer matrix of the nominal plant model is identified, balanced, and order-reduced in the state-space format. The plant modeling uncertainty is obtained by a least-squares fit of the non-parametric model generated by system identification of experimental data via the statistical plant set estimation method of Bayard (1992). Accuracy of the least-squares fit is within 95% statistical confidence. For the sake of completeness, continuous-time versions of discrete-time transfer matrices of the nominal plant model and the frequency-dependent modeling uncertainties that are presented in a previous publication (Zhang & Ray, 1999) are reproduced below:

$$G_{\text{nom}}(s) \Leftrightarrow \begin{cases} \dot{x}(t) = Ax(t) + Bu(t), \\ y(t) = Cx(t) + Du(t), \end{cases} \quad (2)$$

where

$$A = \begin{bmatrix} -12.3344 & -0.2442 & 2.0873 & -45.4482 & -7.2123 & -1.9009 & 0.0297 & 15.0672 \\ 0.2892 & -12.6160 & -45.1486 & 2.9354 & -29.4505 & 9.6131 & -0.6609 & 0.0835 \\ -2.5686 & 43.9109 & -42.4215 & 7.4735 & -27.2888 & 13.5764 & 2.2892 & -7.3930 \\ 44.2971 & -3.3459 & 10.5402 & -91.1235 & -25.6785 & -7.5726 & 14.3289 & 85.2843 \\ 5.7765 & 32.7387 & -61.3690 & -0.0054 & -64.5499 & -45.9878 & -5.3407 & 28.2589 \\ 1.4704 & -11.4701 & 30.0693 & -6.8968 & 96.5308 & -0.4557 & 4.2777 & 9.1054 \\ 0.5287 & 1.5159 & -5.4316 & -5.8283 & -5.8722 & 0.8842 & 11.7917 & -96.4984 \\ 10.3578 & -0.5226 & 6.2207 & -74.8315 & -18.6879 & -4.6380 & 66.2060 & -46.2613 \end{bmatrix},$$

$$C = \begin{bmatrix} 0.0001 & -0.0033 & -0.0232 & -0.0050 & 0.0205 & 0.0069 & 0.0057 & 0.0021 \\ 0.0126 & -0.0588 & -0.0448 & 0.0173 & -0.0367 & 0.0154 & -0.0025 & -0.0049 \\ 0.0634 & 0.0120 & 0.0045 & 0.0667 & 0.0195 & -0.0007 & -0.0037 & -0.0188 \end{bmatrix},$$

$$B = \begin{bmatrix} 3.5093 & 18.9213 \\ -17.2325 & 3.2579 \\ 18.6961 & -1.8578 \\ -6.2382 & -25.0847 \\ 16.6041 & -6.6138 \\ -7.8283 & 0.8071 \\ 0.8360 & -0.5235 \\ -1.9179 & -8.3043 \end{bmatrix}, \text{ and } D = \begin{bmatrix} 0 & 0 \\ 0 & 0 \\ 0 & 0 \end{bmatrix}.$$

The transfer function of the uncertainty weighting matrix in Fig. 4 is fitted from the non-parametric data as

$$W_{del}(s) = \left( \frac{0.017757s^3 + 5.4138s^2 + 73.0835s + 1480.1260}{s^3 + 12.5303s^2 + 1635.4813s + 7606.1516} \right) \times \begin{bmatrix} 1 & 0 \\ 0 & 1 \end{bmatrix}. \quad (3)$$

Note that only one, namely, the displacement  $y_1$  of Mass# 1, of the three plant outputs is regulated with respect to the reference trajectory.

### 5. Linear robust control synthesis

The methodology of robust damage-mitigating control synthesis is initiated with a conventional set-up consisting of a generalized plant model in the top half of Fig. 3 which is obtained with no specific consideration to fatigue damage. Subsequently, as seen in the bottom half of Fig. 3, the conventional set-up is extended to penalize the damage-causing plant variables that are responsible for

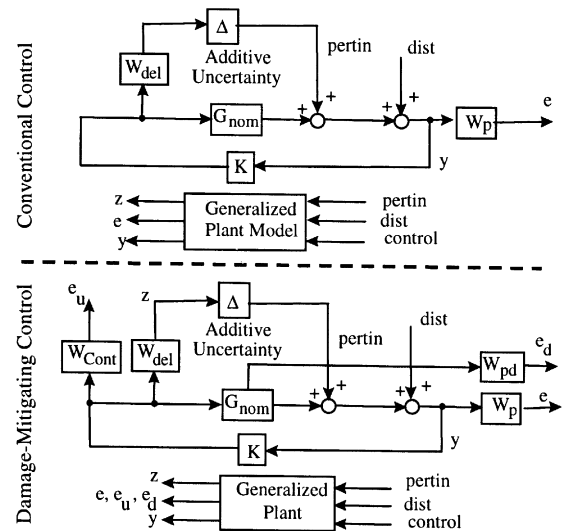


Fig. 3. Conventional and damage-mitigating control.

creating high stresses at the failure site of the test specimen. In both top and bottom halves of Fig. 3,  $G_{nom}(s)$  is the nominal plant model of the test apparatus,  $W_{del}(s)$  is the model of additive uncertainty, and  $\Delta(s)$  is the uncertainty block structure. Note that  $W_p(s)$  is the weight that scales the total performance level so that an achievable controller can be found via  $W_p - \gamma$  iteration (Zhou, Doyle & Glover 1996). Following the  $H_\infty$ -based controller design scheme in the top part of Fig. 3, an internally stabilizing control law  $K_C(s)$  is now formulated by optimization of the robust performance functional in the form given below (Zhou et al., 1996):

$$\min_{K_C} \{ \|F_u(F_1(P_C(s), K_C(s)), \Delta(s))\|_\infty < 1 \} \quad \forall \Delta(s) \text{ with } \|\Delta(s)\|_\infty \leq 1, \quad (4)$$

where  $F_u(\cdot, \cdot)$  and  $F_l(\cdot, \cdot)$  are upper and lower linear fractional transform (LFT) operators, respectively;  $\Delta(s)$  is the block structure of modeling uncertainty represented by a matrix of compatible dimension; and  $P_C(s)$  is the generalized plant model obtained by augmenting the nominal plant model  $G_{\text{nom}}(s)$  with the uncertainty weight  $W_{\text{dei}}(s)$  and the performance weight  $W_p(s)$ . Optimization of the cost functional guarantees loop-shaping relative to the preset weighting matrices  $W_{\text{dei}}(s)$  and  $W_p(s)$ , thereby reaching the goal of uncertainty tolerance and disturbance rejection. The objective at this step is to design a high-quality (i.e., good dynamic performance) controller with no direct consideration of damage mitigation.

Next we penalize, in addition, the pertinent damage-causing variable(s) within the  $H_\infty$ -synthesis structure as shown in the bottom half of Fig. 3. The objectives are now to reduce the amplitude of the dominant *damage-causing* mode in the control signal and, as necessary, change the amplitudes of other modes to circumvent the (possible) loss of performance. Relative to the experiments on the test apparatus in Fig. 2, we make the following two observations:

- The first mode is responsible for resonant vibrations and hence dominates the damage process because the failure site is subjected to higher stress amplitudes with larger vibration of the free Mass #3. Penalizing this resonant mode does not strongly affect the system performance (i.e., tracking ability of Mass #1 and Mass #2).
- The displacement of Mass #3 is not a performance variable and is not directly controlled by any one of the two actuators but its motion significantly affects the stress amplitude at the failure site.

The robust controller is now designed based on the above two physical phenomena by including three additional variables that are the displacement,  $y_3$ , of Mass #3 and the two control inputs (i.e., signals exciting the actuators),  $u_1$  and  $u_2$ . The estimated far-field stress  $\hat{S}$  at the failure site (obtained as a linear combination of the displacements,  $y_1, y_2$ , and  $y_3$ , via Eq. (1)) and both control inputs,  $u_1$  and  $u_2$ , are penalized by frequency-dependent weights,  $W_{\text{pd}}(s)$  and  $W_{\text{cont}}(s)$ , respectively. Following the damage-mitigating procedure in the bottom part of Fig. 3, an internally stabilizing  $H_\infty$  control law  $K_{\text{DMC}}(s)$  is formulated and solved to optimize the robust performance in the form given below:

$$\min_{K_{\text{DMC}}} \{ \|F_u(F_l(P_{\text{DMC}}(s), K_{\text{DMC}}(s)), \Delta(s))\|_\infty < 1 \} \\ \forall \Delta(s) \text{ with } \|\Delta(s)\|_\infty \leq 1 \}, \quad (5)$$

where  $F_u(\cdot, \cdot)$ ,  $F_l(\cdot, \cdot)$ , and  $\Delta(s)$  are the same as defined in Eq. (4); and  $P_{\text{DMC}}(s)$  is the generalized plant model obtained by augmenting the nominal plant model  $G_{\text{nom}}(s)$

with the uncertainty weight  $W_{\text{dei}}(s)$  and the performance weights  $W_p(s)$ ,  $W_{\text{pd}}(s)$ , and  $W_{\text{cont}}(s)$  following the bottom part of Fig. 3. Note that the damage-mitigating controller  $K_{\text{DMC}}(s)$ , generated from Eq. (5), is of higher order than the conventional controller  $K_C(s)$ , generated from Eq. (4), because  $P_{\text{DMC}}(s)$  is of higher order than  $P_C(s)$  due to dynamics of the additional performance weights. The performance weighting matrices in Fig. 3 are

$$W_p(s) = \left[ \frac{0.4s + 50}{s + 1} \right], \quad (6)$$

$$W_{\text{cont}}(s) = \left( \frac{0.036546s^2 + 1.7443s + 0.72237}{s^2 + 22.5166s + 1873.133} \right) \begin{bmatrix} 1 & 0 \\ 0 & 1 \end{bmatrix}, \quad (7)$$

$$W_{\text{pd}}(s) = [0.1]. \quad (8)$$

In Eq. (6), the transfer function  $W_p$  of is a low-pass filter that penalizes the low-frequency part of the tracking error to ensure a good steady-state response. In Eq. (7), the transfer function of  $W_{\text{cont}}$  is a band-pass filter that penalizes the control input within a frequency range to suppress the resonant vibration. In Eq. (8),  $W_{\text{pd}}$  is an all-pass filter that penalizes, over the entire frequency range, the displacement of Mass #3 which is not directly controlled by any one of the two actuators but is responsible for causing stresses at the failure site.

## 6. Damage status evaluation and discrete-event supervisory control

This section presents the remaining two major functional modules of the hybrid life-extending control system: *Damage Status Evaluator* and the *Discrete-Event Supervisory controller*. Since the linear control system in Section 5 is designed to be robustly stable, the plant performance can be made to be bounded by constraining the output of the plant performance generator as norm-bounded. The critical question on stability that remains to be answered is oscillatory behavior (e.g., limit cycling) of the closed-loop control system.

### 6.1. Convergence of the reinforcement scheme in the damage status evaluator

The reward/penalty functions of the damage status evaluator are realized by the reinforcement scheme of a variable-structure stochastic automaton (VSSA). The VSSA is represented by the triple  $\{U, \psi, A\}$  where the action  $u(\cdot)$  is exactly one element of the (non-empty) set  $U = \{u_1, u_2, \dots, u_r\}$  of available action events; the damage status  $\psi[-1, 1]$  is the set of response serving as the S-model input to the VSSA; and  $A: U \times \psi \rightarrow U$  is realized

by the (dynamic) reinforcement scheme that generates probabilities of the individual action events. The value of  $\psi$  indicates the level of damage increment where  $\psi \rightarrow 0$  means that the actual damage increment is close to what is desired and  $\psi \rightarrow \pm 1$  means that the actual damage measure is far from the desired value in positive or negative direction, respectively.

The input  $\psi$  is obtained, at selected time epochs, as an algebraic function of: (i) the damage increment set point  $\delta D_{\text{set}}$  which is derived, via the D/C interface, from the mission objectives; and (ii) the damage increment  $\delta D \geq 0$  which is a continuous function of measured plant output variables  $y^{\text{dam}}$ . The statistics of fatigue crack damage  $D$  and damage increment  $\delta D$  are shown by Ray (1999) to be approximately lognormal-distributed. The stochastic model of damage is summarized in Appendix B. Given the probability distribution function  $F(\cdot)$  of  $\delta D$ , (analytic) measurements of  $E[\delta D]$ , and the specified reference  $\delta D_{\text{set}}$ , the damage status  $\psi$  is defined as follows:

$$\psi \equiv \begin{cases} \frac{F(\delta D_{\text{set}}) - F(E[\delta D])}{1 - F(E[\delta D])} & \text{if } \delta D_{\text{set}} \geq E[\delta D], \\ \frac{F(\delta D_{\text{set}}) - F(E[\delta D])}{F(E[\delta D])} & \text{if } E[\delta D_{\text{set}}] \leq E[\delta D]. \end{cases} \quad (9)$$

Note that the damage status  $\psi$  is an input to the reinforcement scheme and its definition in Eq. (9) captures the stochastic nature of crack growth increment. The set  $U$  of action events must be chosen before constructing the reinforcement scheme. In this application,  $U$  is selected as

$$U = \{\text{No Action, Reduce Performance, Increase Performance}\} \quad (10)$$

with the number of actions  $r = 3$ . In general, a viable linear reward–penalty reinforcement scheme for the S-model ( $SL_{\text{RP}}$ ) is

$$p_j(n+1) = \begin{cases} p_j(n) + \psi(n)[a/(r-1) - ap_j(n)] - [1 - \psi(n)]ap_j(n) & \text{for } u(n) \neq u_j, \\ p_j(n) - \psi(n)ap_j(n) + [1 - \psi(n)]a(1 - p_j(n)) & \text{for } u(n) = u_j, \end{cases} \quad (11)$$

where  $a$  is a constant parameter; and  $\mathbf{p}(n) = [p_1(n) \ p_2(n) \ \cdots \ p_r(n)]^T$  is the probability vector of individual actions (i.e.,  $p_j(n) \equiv \text{Pr}[u(n) = u_j]$ ) and is constrained by

$$\sum_{k=1}^r p_k(n) = 1 \quad \forall n \quad \text{and} \quad p_j(n) \geq 0 \quad \forall n \quad \text{for } j = 1, 2, \dots, r. \quad (12)$$

**Theorem 1.** *The  $SL_{\text{RP}}$  reinforcement scheme in Eq. (10) converges regardless of the initial value  $\mathbf{p}(0)$ .*

**Proof.** The theorem is stated by Narendra and Thathachar (1989) without proof. A proof is presented below.

Defining  $s_i \equiv E[\psi(n)|u(n) = u_i]$ , it follows that

$$\begin{aligned} E[p_j(n+1)|\mathbf{p}(n), \psi(n)] &= [p_j(n) + a - as_j - ap_j(n)]p_j(n) \\ &+ \sum_{k \neq j}^r \left[ p_j(n) + \frac{as_j}{r-1} - ap_j(n) \right] p_k(n) \\ &= (1 - as_j)p_j(n) + \sum_{k \neq j}^r \frac{as_k}{r-1} p_k(n). \end{aligned} \quad (13)$$

Taking expectation on both sides of Eq. (12) and using the property  $E[Y] = E[E[Y|X]]$ , we obtain

$$E[\mathbf{p}(n+1)] = C^T E[\mathbf{p}(n)], \quad (14)$$

where  $c_{ii} \equiv 1 - as_i$  and  $c_{ji} \equiv as_j/(r-1) \ \forall i \neq j$ . The solution of Eq. (13) yields  $\lim_{n \rightarrow \infty} E[p_i(n)] = 1/s_i / \sum_{i=1}^r (1/s_i)$ .  $\square$

**Remark 1.** Focusing on the lower tier of the hybrid control system only, Theorem 1 establishes that the  $SL_{\text{RP}}$  reinforcement scheme converges regardless of the initial value of probabilities of the individual actions.

So far as oscillatory instability of the performance set point is concerned, there are two potential problems:

- If the step to increase or decrease the performance level is too large, then the control system tends to chatter between the actions of increase and decrease.
- If the step to increase or decrease the performance level is too small, then it may take a significantly long period to reach the steady state.

Discrete-event supervisory control is a viable option for circumventing the above problems. The approach is to identify an event string for selection of a sequence of steps where the output actions resulting from the reinforcement schemes can be translated by the C/D interface as input events to the supervisory controller. In this case, the supervisory controller will have the authority of regulating the event strings to update the performance set point.

## 6.2. Discrete-event supervisory controller

A discrete-event model of the controlled plant is now formulated for synthesizing the supervisory controller. Following Ramadge and Wonham (1987), the discrete-event plant model is formulated in the format of a quintuple automaton defined as  $M = \langle Q, \Sigma, \delta, q_0, F \rangle$  where  $Q$  is

the set of plant states  $q$ ,  $\Sigma$  is the finite set of events; the transition function  $\delta: \Sigma \times Q \rightarrow Q$  is a partial function,  $q_0 \in Q$  is the initial state, and  $F \subset Q$  is a subset of states that only contain the *marked states*. The formulation of the discrete-event plant model depends not only on the physical process but also on the specifications of the discrete-event controller. In the present case, the role of the discrete-event controller is limited to prevention of oscillatory instability and avoidance of sluggish behavior of the physical process. Therefore, the continuously varying controller at the lower tier operates more or less autonomously and only the set points of damage increment and performance need to be specified. Accordingly, the set of states  $Q = Q_1 \times Q_2$  of the discrete-event controller are defined as

$$Q_1 = [\text{OK}, \text{High}, \text{Low}],$$

$$\begin{aligned} \text{Low: } & \psi \in [-1, -0.1], \\ \text{OK: } & \psi \in [-0.1, 0.1], \\ \text{High: } & \psi \in [0.1, 1], \end{aligned}$$

$$Q_2 = \{1, \frac{1}{2}, 2\},$$

- 1: Maintaining the step size unchanged,
- $\frac{1}{2}$ : Reducing the step size in half,
- 2: Doubling the step size,

$\Sigma = \Sigma_c \cup \Sigma_u$  is the event set having:

$\Sigma_c := \{R, I, D, H\}$  is the set of controllable events where R and I are derived by the C/D interface from the output of the reinforcement scheme, and D and H are generated by the discrete-event supervisory controller (Stiver et al., 1995):

- R Reducing the performance set-point by one step of current size;
- I Increasing the performance set-point by one step of current size;
- D Doubling the current step size of the performance set-point;
- H Halving the current step size of the performance set-point.

$\Sigma_u := \{\alpha, \beta, \gamma\}$  is the set of uncontrollable events that is a combination of the sensory information (i.e.,  $y^{\text{per}}$  and  $y^{\text{dam}}$ ) on the physical process and the qualitative information on mission objectives:

- $\alpha$ : the current damage increment is allowable;
- $\beta$ : the current damage increment is high;
- $\gamma$ : the current damage increment is low.

**Remark 2.** The discrete-event plant model  $M = \langle Q, \Sigma, \delta, q_0, F \rangle$  captures the physics of plant dynamics in an abstract manner and is also responsive to the commands issued by the supervisory controller.

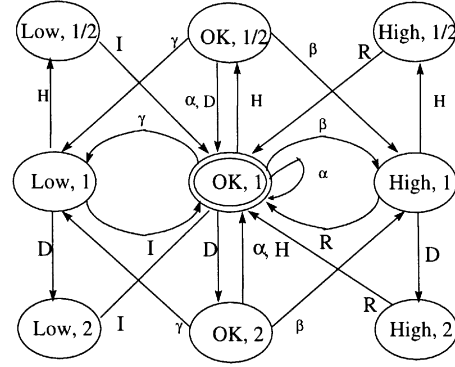


Fig. 4. Transition graph of the discrete-event plant model.

Referring to the state transition function of the discrete-event plant model in Fig. 4, the language of the plant behavior may now be expressed as

$$L(G) = pr[(\alpha + \beta R + \gamma I)^*(H(D + (\alpha + \beta R + \gamma I)^*))^* + D(H + (\alpha + \beta R + \gamma I)^*)^*] \quad (15)$$

and the marked language is

$$L_m(G) = (\alpha + \beta R + \gamma I)^*(H(D + (\alpha + \beta R + \gamma I)^*))^* + D(H + (\alpha + \beta R + \gamma I)^*)^*. \quad (16)$$

The specifications for the desired language  $K$  are stated as follows:

- For any sub-trace  $(\beta R \gamma I)^N$  or  $(\gamma I \beta R)^N$  to belong to  $K$  where  $N$  is specified be less than 3 in this case.
- For any sub-trace  $(\beta R)^N$  or  $(\gamma I)^N$  to belong to  $K$  where  $N$  is specified to be less than 3 in this case.

**Remark 3.** A physical interpretation of the marked language  $L_m(G)$  is that the supervisor, if it exists, would lead the system to the marked state  $\{\text{OK}, 1\}$ . In other words, the closed-loop system would attempt to limit the damage-increment in the critical component(s) as defined in the mission objective(s). Kumar and Garg (1995, p. 68) have shown that the requirement of marked behavior leads to  $\Sigma_u$ -enabling, non-marking and non-blocking properties of the synthesized supervisor.

**Remark 4.** If the  $\{\text{OK}, 1\}$  state is maintained, the current damage increment and performance set-points are appropriate for the mission objectives and operating status of the physical plant. Otherwise, either  $\beta$  or  $\gamma$  bring the model to a non-OK state. Then, the events *reduce* (R) and *increase* (I) adjust the performance set-point to control the plant operation so that the plant status is brought back to the  $\{\text{OK}, 1\}$  state. If the plant behavior is oscillatory or very slowly converging, the supervisory controller automatically adjusts the performance step such that the undesirable behavior is avoided.

The specification  $K$  is expressed as a state machine shown in Fig. 5. It can also be shown that  $K$  is controllable and  $K = pr(K) \cap L_m(G)$ . The discrete-event supervisor  $S$  is chosen as  $L_m(S) = L(S) = pr(K)$  following (Kumar & Garg, 1995) and is executed using a software package by Sanghavi and Garg (1991). Existence of the supervisory control law has been checked and the results show that there is no uncontrollable transition from *good states* to *bad states*. Therefore, the supervisor is chosen to be the same as  $K$ .

**Remark 5.** Stability of the hybrid control system in Fig. 1 depends on the linear robust control law and the switching policy of the nonlinear reinforcement scheme at the lower tier and the discrete-event supervisor algorithm at the upper tier. The robust controller guarantees local stability if uncertainties and disturbances are confined within the allowable bound. Therefore, the hybrid control system remains norm-bounded because the output of the plant performance set-point generator is constrained. Convergence of the reinforcement scheme of the learning automaton in Theorem 1 ensures that the switching actions steer the set-point changes in the correct direction. Interactions of the discrete-event supervisor with the linear control system take place (via the D/C interface) only by changes in the performance set point that serves as a time-dependent reference trajectory. Therefore, only possible instability in the plant dynamics is chattering caused by the switching of the performance set point. This issue is addressed in the specifications of supervisory controller at the upper tier, which is designed to eliminate potential oscillations in the performance set-point. Experimental results are presented in the next section to validate this claim. Note that this concept of stability in the physical plant under hybrid control is different from that of discrete-event system stability as

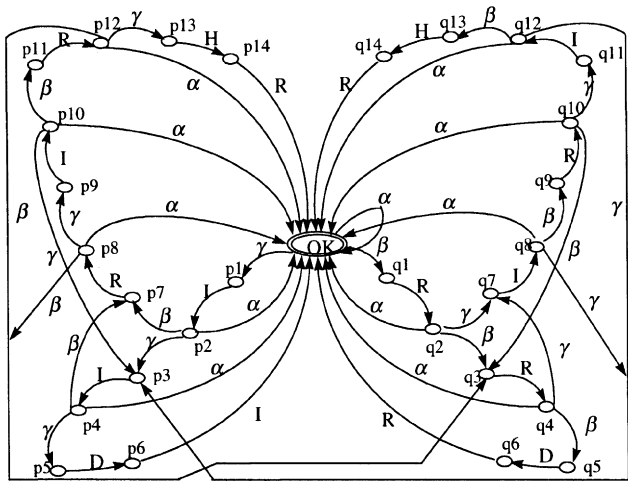


Fig. 5. State machine for specifications and the discrete-event supervisor.

defined in terms of legal behavior by other investigators (e.g., Kumar, Garg & Marcus, 1993; Passino, Michel & Antsaklis, 1994; Burgess & Passino, 1995). In these cases, the system is initially allowed to make illegal transitions but, after a finite number of transitions, the supervised system makes only legal transitions. While the present paper does not specifically address the issue of legal and illegal transitions, it focuses on robust stability and performance including prevention of undesirable chattering and oscillations in the plant variables.

### 7. Experimental results and discussion

The robust damage-mitigating control law is implemented in discrete-time form on a Pentium processor that is a part of the instrumentation & control system of the test apparatus. The sampling time is chosen to be 2.516 ms so that 192 sampled data points form a cycle of 2.07 Hz that is one-third of the resonance frequency 6.21 Hz. The two-input single-output plant dynamics of the test apparatus are now investigated where the performance specifications require tracking ability of the regulated output (i.e., displacement of Mass#1) by manipulation of both actuators. Fig. 6 presents a comparison of the displacement profile of Mass#1 in response to a (square-wave) reference when the test apparatus is operated under: (i) the conventional controller; and (ii) the damage-mitigating controller. While dynamic performance of the damage-mitigating controller is almost identical to that of the conventional controller, the fatigue life of the test specimen is increased by a factor of  $\sim 20$  as seen in Fig. 7. This shows that if redundant actuators are available, a damage-mitigating control system can be designed to yield large savings in structural durability with no appreciable loss of performance.

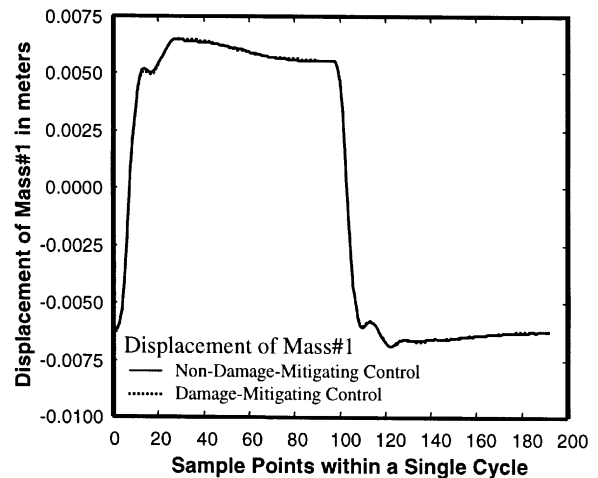


Fig. 6. Performance comparison for the regulated output.

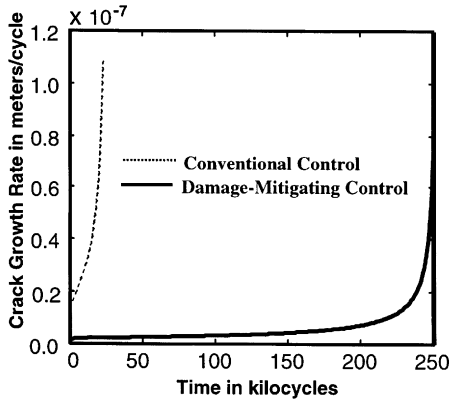


Fig. 7. Comparison of fatigue crack growth rate.

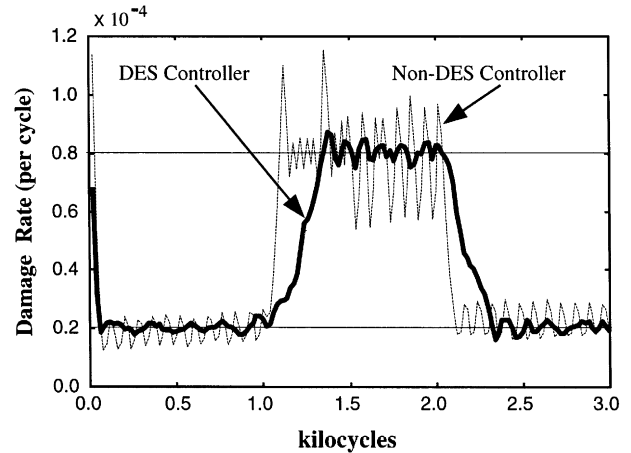


Fig. 9. Experiment Set #2 with and without discrete-event supervisory control.

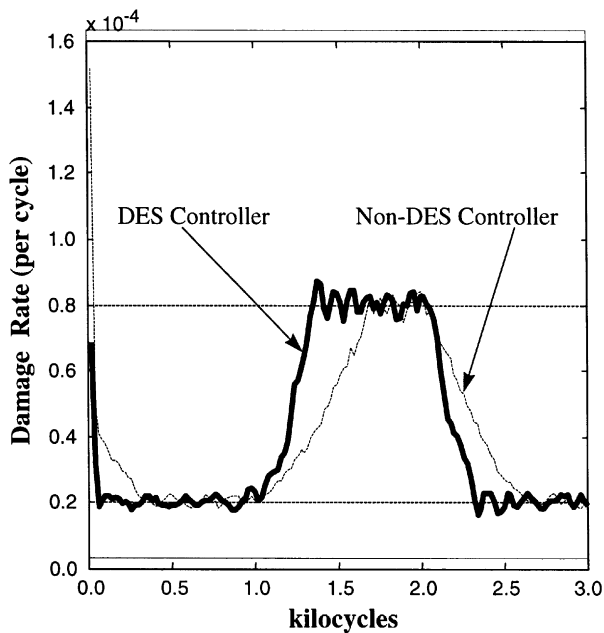


Fig. 8. Experiment Set #1 with and without discrete-event supervisory control.

To demonstrate the effectiveness of the proposed hybrid control scheme, each experiment is conducted on the test apparatus with two controllers: one with the discrete-event supervisor, referred to as *DES Controller*, and the other without the discrete-event supervisor, referred to as *Non-DES Controller*. The DES and non-DES controllers are excited with identical command inputs in each set of experiments. The initial damage increment set point is  $2 \times 10^{-5}$  per cycle up to 1000 cycles, then increased to  $8 \times 10^{-5}$  per cycle, and subsequently changed back to  $2 \times 10^{-5}$  per cycle at 2000 cycles. The step size of the performance set-point is varied by the DES controller and it is held fixed at 0.001 for the Non-DES controller in the experiment set #1. Fig. 8 shows that the overall response time of the DES controller is faster than that of

the Non-DES controller that requires a larger number of relatively small fixed-size steps. The superior performance of the DES controller results from smaller delays as the step size is automatically adjusted. The experiment set #2 in Fig. 9 is carried out to compare robust stability of the DES and Non-DES controllers if the fixed step size of the Non-DES controller happens to be too large. The command inputs for both control systems are kept identical to those for the experiment set #1 in Fig. 8 except that the fixed step size of the performance set-point for the Non-DES controller is now increased ten-fold to 0.01. Fig. 9 demonstrates that, with this fixed large step size, the response of the Non-DES controller becomes oscillatory around the reference signal while the DES controller has the ability to automatically adjust the step size so that the oscillations are eliminated at the expense of somewhat sluggish response. Figs. 8 and 9 exhibit the advantages of discrete-event supervisory control in terms of both stability and performance.

## 8. Summary and conclusions

This paper presents a design concept and a two-tier architecture for hybrid life extending control of mechanical systems. The methodology for control systems analysis and synthesis is based on the principles of robust  $H_\infty$  control, variable-structure stochastic automaton, and supervisory discrete-event control. The concept and a design methodology for damage-mitigating control have been experimentally validated on a test apparatus that is constructed on a three degree-of-freedom vibrating structure to emulate an operating machinery. The linear controller at the lower tier is designed based on  $H_\infty$ -optimization with due consideration to robust performance and damage mitigation. The methodology

also includes the usage of a novel frequency-domain technique to identify both a nominal model of plant dynamics and the associated additive uncertainty weight for robust controller design. The decisions of on-line adjustment of the performance set point are made based on variable-structure stochastic automaton, and supervisory discrete-event control.

Experiments on the test apparatus demonstrate that fatigue life of critical plant components can be substantially extended with no appreciable degradation in the dynamic performance of the mechanical system. In particular, if redundant actuators are available, it is possible to design a control system that would yield large savings in structural durability with no appreciable loss of dynamic performance. This is a clear message that the consideration of damage in the control of transients to which an operating machinery is subjected can have a significant impact on the life of critical components. If one is willing to pay a small price in loss of dynamic performance and/or installation of redundant actuators, much larger gains in structural durability can be achieved.

The results of experimentation on the test apparatus also show that the dynamic response time of the plant variables is significantly improved with the discrete-event controller. In the proposed approach, the supervisory control algorithm in the upper tier is formulated in terms of the damage increment and performance set points in the discrete-event setting while the continuously varying part of the control system in the lower tier is executed autonomously. These two parts of the hybrid control system are interfaced following the concept of classical feedback control. The discrete-event supervisor is capable of generating commands as control patterns to mandate any changes in the performance set-point based on the information received from the sensor data and the reinforcement scheme of the variable-structure stochastic automaton.

## Acknowledgements

The authors acknowledge beneficial of technical discussions with Professor Marc Carpino at Pennsylvania State University and Professor Ratnesh Kumar at University of Kentucky.

## Appendix A. Deterministic state-space modeling of fatigue crack growth

The fatigue crack growth model under consideration is represented by a nonlinear difference equation in which the crack increment during the  $k$ th cycle is obtained as a function of the maximum applied remote stress

$S_k^{\max}$  and the crack opening stress  $S_k^o$  as

$$\hat{c}_k = \hat{c}_{k-1} + \hat{\Omega} (\Delta K_k^{\text{eff}})^m \quad \text{for } \hat{c}_0 > 0,$$

$$\Delta K_k^{\text{eff}} = \Delta S_k \sqrt{\pi \hat{c}_{k-1}} F(\hat{c}_{k-1}), \quad (\text{A.1})$$

$$\Delta S_{k-1} = S_k^{\max} - S_{k-1}^o.$$

where  $\hat{c}_k$  is the sum of the (estimated) mean crack length and the plastic zone radius at the end of the  $k$ th cycle,  $\Delta S_k$  the effective stress range,  $\Delta K_k^{\text{eff}}$  is the effective stress intensity factor range that is a function of,  $F$  is the correction factor for finite geometry of the specimen; and  $\hat{\Omega}$  and  $m$  are material constants. A cycle ranges from a minimum stress to the next immediate minimum stress. If the frequency and shape effects are negligible (e.g., for aluminum and ferrous alloys at room temperature), a stress cycle is defined by the maximum stress  $S^{\max}$  and the minimum stress  $S^{\min}$  that follows. Crack opening stress  $S_k^o$  is governed by the following difference equation (Patankar et al., 1998):

$$\begin{aligned} S_k^o = & \left( \frac{1}{1+\eta} \right) S_{k-1}^o + \left( \frac{\eta}{1+\eta} \right) S_k^{\text{oss}} \\ & + \left( \frac{\lambda_k}{1+\eta} \right) (S_k^{\text{oss}} - S_{k-1}^o) U(S_k^{\text{oss}} - S_{k-1}^o), \end{aligned} \quad (\text{A.2})$$

where

$$R_k = \frac{S_k^{\text{mod}}}{S_k^{\text{max}}}, \quad S_k^{\text{mod}} = \frac{\alpha S_k^{\min} + S_{k-1}^{\min}}{\alpha + 1},$$

$$S_k^{\text{oss}} = (A_0 + A_1 R_k + A_2 R_k^2 + A_3 R_k^3) S_k^{\text{max}},$$

$$A_0 = (0.825 - 0.34\alpha + 0.05\alpha^2) \left[ \cos \left( \frac{\pi S_k^{\text{max}}}{2 S_k^{\text{flow}}} \right) \right]^{1/\alpha},$$

$$A_1 = (0.415 - 0.071\alpha) \left( \frac{S_k^{\text{max}}}{S_k^{\text{flow}}} \right),$$

$$A_2 = \begin{cases} 1 - A_0 - A_1 - A_3 & \text{if } R_k > 0, \\ 0 & \text{if } R_k \leq 0, \end{cases}$$

$$A_3 = \begin{cases} 2A_0 + A_1 - 1 & \text{if } R_k > 0, \\ 0 & \text{if } R_k \leq 0, \end{cases}$$

$$\lambda_k = \left( \frac{S_k^{\text{max}} - S_k^{\text{mod}}}{S_k^{\text{max}} - S_{k-1}^{\min}} \right), \quad U(x) := \begin{cases} 0 & \text{if } x \leq 0, \\ 1 & \text{if } x > 0, \end{cases}$$

$\eta$  = decay constant,

$$S_k^{\text{flow}} = \frac{\sigma_{\text{yield}} + \sigma_{\text{uts}}}{2},$$

where  $\sigma_{\text{yield}}$  is the yield stress,  $\sigma_{\text{uts}}$  is the ultimate strength, and  $\alpha$  is the constraint factor (1 for plane stress and 3 for plane strain).

Table 1  
Mechanical properties of 6063-T6 aluminum alloy (Kumar, 1990)

$\sigma_{ys}$ (MPa)	$\sigma_{ult}$ (MPa)	Elongation (%)	Reduction in area (%)	Young's modulus (MPa)	Strain hardening exponent
201	230	15.84	57.12	$72 \times 10^3$	0.06

Table 2  
Model parameters for crack growth and crack opening stress of 6063-T6 aluminum alloy

$\hat{\Omega} = 0.62 \times 10^{-12}$	$m = 3.8$	$\alpha = 1.6$	$\eta = 2 \times 10^{-4}$	$w = 6.251 \times 10^{-3}$ m
---------------------------------------	-----------	----------------	---------------------------	------------------------------

The transients of the crack opening stress  $S_k^o$  after a single overload display immediate increment and decay at a slow rate. Since the difference  $\Delta S_k = S_k^{\max} - S_{k-1}^o$  determines the effective crack growth rate as seen in Eq. (A.1), the consequence of an overload is a decrease in the crack growth rate. Physical explanation of this phenomenon can be found in Suresh (1991) Patankar et al. (1998). Eqs. (A.1) and (A.2) together constitute a dynamical model of fatigue crack growth where the state variables are  $\hat{c}_k$  and  $S_k^o$ .

The material of the specimen at the failure site in Beam #2 of the test apparatus in Fig. 2 is 6063-T6 aluminum alloy. The geometry factor is assumed to be proportional to that for center-cracked specimens, i.e.,  $F = \sqrt{\sec(\pi\hat{c}_{k-1}/(2w))}$ . The material parameters of 6063-T6 are listed in Table 1 and the model parameters used in Eqs. (A.1) and (A.2) are given in Table 2.

## Appendix B. Stochastic modeling of fatigue crack damage (Ray, 1999)

The stochastic continuous-time model of fatigue crack growth is built upon the structure of the mean-value discrete model described in Appendix A. Given the geometry factor  $F = \sqrt{\sec(\pi\hat{c}(t)/(2w))}$  for center-cracked specimens of half-width  $w$ , Eq. (A.1) is modified via series approximation of the  $(m/2)$ th power of the secant term:

$$\delta\hat{c}(t) = \hat{\Omega}\Delta S(t)^m \hat{c}(t)^{m/2} \left(1 - m\left(\frac{\pi}{4w}\right)^2 \hat{c}(t)^2\right)^{-1} \delta t, \quad t \geq t_0 \text{ and given } \hat{c}(t_0) > 0, \quad (\text{B.1})$$

where  $t$  is the current time upon completion of a stress cycle, and  $t_0$  is the initial time (e.g., when the machine component is put in service after a major maintenance or inspection),  $\hat{c}(t)$  is the estimated mean value of (time-dependent) crack length,  $\delta\hat{c}(t)$  is the increment of the estimated mean crack length over one cycle after time  $t$ , and  $\delta t$  indicates the time increment over that cycle, and

$\Delta S(t)$  is the effective stress range during one cycle (after time  $t$ ) with the corresponding crack opening stress  $S^o(t)$  and peak stress  $S^{\max}(t)$ . For constant-amplitude load, Eq. (B.1) reduces to the well-known Paris equation (Suresh, 1991).

Statistical analysis of the experimental data (for 2024-T3 and 7075-T6 aluminum alloys) reveals that the random exponent  $m(\zeta)$  can be approximated as a constant for all specimens (i.e.,  $m(\zeta) = m$  with probability 1) at different levels of constant stress range  $\Delta S$  for a given material. Based on this observation and the (deterministic) model structure in Eq. (B.1), Ray (1999) postulated and validated the following constitutive equation for fatigue crack growth in the stochastic setting:

$$\delta c(\zeta, t) = \Omega(\zeta, \Delta S(t)) (\Delta S(t))^m c(\zeta, t)^{m/2} \left(1 - m\left(\frac{\pi}{4w}\right)^2 c(\zeta, t)^2\right)^{-1} \rho(\zeta, t) \delta t, \quad t \geq t_0 \text{ and given } c(\zeta, t_0) > 0, \quad (\text{B.2})$$

where the random process  $\Omega(\zeta, \Delta S)$  represents uncertainties of a test specimen  $\zeta$  for a stress range  $\Delta S$  (i.e.,  $\Omega$  is a constant for a given specimen under a given stress range); the noise process  $\rho(\zeta, t)$  represents the uncertainties in material microstructure and crack-length measurements that vary with  $t$  as the crack propagates even for the same specimen  $\zeta$ . The multiplicative uncertainty  $\rho(\zeta, t)$  in the crack growth process is assumed to be a white stationary process which is statistically independent of  $\Omega(\zeta, \Delta S)$ . The rationale for this assumption is that inhomogeneity of the material microstructure and measurement noise associated with each test specimen, represented by  $\rho(\zeta, t)$ , are statistically homogeneous and are unaffected by the uncertainty  $\Omega(\zeta, \Delta S)$  of a particular specimen caused by, for example, machining operations. With no loss of generality,  $\mu_\rho \equiv E[\rho(\zeta, t)] = 1$  is set via appropriate scaling of the parameters in Eq. (B.2).

Since the number of cycles to failure is usually very large in the crack growth processes (even for low-cycle fatigue), a common practice in the fracture mechanics literature is to approximate the difference equation of

crack growth by a differential equation. Therefore, for  $t \geq t_o$ , the difference equation (B.2) is expressed as

$$\begin{aligned} & \left( c(\zeta, t)^{-m/2} - m \left( \frac{\pi}{4w} \right)^2 c(\zeta, t)^{2-m/2} \right) dc(\zeta, t) \\ & = \Omega(\zeta, \Delta S(t)) (\Delta S(t))^m \rho(\zeta, t) \delta t, \quad t \geq t_o \\ & \text{and given } c(\zeta, t_o) \end{aligned} \quad (\text{B.3})$$

which is integrated pointwise (i.e., for the individual  $\zeta$ 's) as follows:

$$\begin{aligned} & \int_{c(\zeta, t_o)}^{c(\zeta, t)} \frac{d\zeta}{\zeta^{m/2}} - m \frac{\pi}{4w} \int_{c(\zeta, t_o)}^{c(\zeta, t)} \frac{d\zeta}{\zeta^{-2+m/2}} \\ & = \int_{t_o}^t d\tau \Omega(\zeta, \Delta S(t)) (\Delta S(t))^m \rho(\zeta, \tau) \quad \text{given } c(\zeta, t_o) \end{aligned} \quad (\text{B.4})$$

to yield

$$\begin{aligned} & \left( \frac{c(\zeta, t)^{1-m/2} - c(\zeta, t_o)^{1-m/2}}{1-m/2} \right) \\ & - m \left( \frac{\pi}{4w} \right)^2 \left( \frac{c(\zeta, t)^{3-m/2} - c(\zeta, t_o)^{3-m/2}}{3-m/2} \right) \\ & = \int_{t_o}^t d\tau \Omega(\zeta, \Delta S(t)) (\Delta S(\tau))^m \rho(\zeta, \tau). \end{aligned} \quad (\text{B.5})$$

Note that, for ductile alloys and most metallic materials, the constant parameter,  $m$ , lies between 2.5 and 4 (Suresh, 1991). Hence, it is guaranteed that  $(1-m/2) < 0$  and  $(3-m/2) > 0$  in Eq. (B.5). Let us define the measure of fatigue crack damage and its increment as

$$\begin{aligned} D(\zeta, t, t_o) & \equiv \left( \frac{c(\zeta, t)^{1-m/2} - c(\zeta, t_o)^{1-m/2}}{1-m/2} \right) \\ & - m \left( \frac{\pi}{4w} \right)^2 \left( \frac{c(\zeta, t)^{3-m/2} - c(\zeta, t_o)^{3-m/2}}{3-m/2} \right), \end{aligned} \quad (\text{B.6})$$

$$\delta D(\zeta, t, t_o) = \Omega(\zeta, \Delta S(t)) (\Delta S(t))^m \rho(\zeta, t) \delta t. \quad (\text{B.7})$$

Based on the fatigue test data sets of Virkler, Hillberry and Goel (1979), Ghonem and Dore (1987), and Ghonem and Zeng (1989), it is hypothesized that the random process  $\Omega(\zeta, \Delta S)$  is two-parameter ( $r = 2$ ) lognormal-distributed. The goodness-of-fit of hypothesis is tested by both  $\chi^2$  and Kolmogorov–Smirnov tests. Each of the data sets is partitioned into  $L = 12$  segments to assure that each segment contains at least five samples. With  $(L - r - 1) = 9$  degrees of freedom, the  $\chi^2$ -test shows that, for each of the four data sets, the hypothesis of two-parameter lognormal-distribution of  $\Omega(\zeta, \Delta S)$  passed the 10% significance level which suffices the conventional standard of 5% significance level. For each of the data sets, the hypothesis of two-parameter lognormal-distribution of  $\Omega(\zeta, \Delta S)$  also passed the 20% significance level of the Kolmogorov–Smirnov test.

Since the crack length and crack-growth increment are guaranteed to be non-negative, Eq. (B.3) enforces that the random noise  $\rho(\zeta, t)$  must also be non-negative for all  $\zeta$  and  $t$ . As a viable option, one may hypothesize the two-parameter lognormal distribution for  $\rho(\zeta, t)$  similar in structure to that of  $\Omega(\zeta, \Delta S)$ . Then, the right-hand side of Eq. (B.8) becomes lognormal-distributed because the product of two lognormal variables is lognormal. Details of the statistical analysis and dependence of the statistical parameters on the effective stress range  $\Delta S$  are reported by Ray (1999) and Ray and Patankar (1999).

## References

- Bayard, D. S. (1992). Statistical plant set estimation using Schroeder-phased multisinusoidal input design. *Proceedings of the American control conference*, Vol. 4 (pp. 2988–2995).
- Bayard, D. S. (1993). Frequency domain approach to identification, uncertainty characterization and robust control design. *Proceedings of the IEEE conference on decision and control*, Vol. 3 (pp. 2266–2271).
- Burgess, K. L., & Passino, K. M. (1995). Stability analysis of load balancing systems. *International Journal of Control*, 61(2), 357–393.
- Dai, X., & Ray, A. (1996). Damage-mitigating control of a reusable rocket engine: Parts I and II. *ASME Journal of Dynamic Systems, Measurement, and Control*, 118(33), 401–415.
- Garcia, H. E., & Ray, A. (1996). State-space supervisory control of reconfigurable discrete-event systems. *International Journal of Control*, 63(4), 767–797.
- Ghonem, H., & Dore, S. (1987). Experimental study of the constant probability crack growth curves under constant amplitude loading. *Engineering Fracture Mechanics*, 27, 1–25.
- Ghonem, H., & Zeng, M. (1989). *Probability description of fatigue crack growth under constant and variable amplitude loading*. Wright Patterson Report No. AFOSR-TR-89-0716.
- Holmes, M., & Ray, A. (1998). Fuzzy damage mitigating control of mechanical structures. *ASME Journal of Dynamic Systems, Measurement and Control*, 120(2), 249–256.
- Kallappa, P. T., Holmes, M., & Ray, A. (1997). Life extending control of fossil power plants for structural durability and high performance. *Automatica*, 33(6), 1101–1118.
- Kumar, R. (1990). Experimental observation of crack propagation in 6063-T6 Al-alloy under constant amplitude loading. *International Journal of Pressure Vessel & Piping*, 42, 303–315.
- Kumar, R., Garg, V. K., & Marcus, S. I. (1993). Language stability and stabilizability of discrete event dynamical systems. *SIAM Journal of Control and Optimization*, 31(5), 1294–1320.
- Kumar, R., & Garg, V. K. (1995). *Modeling and control of logical discrete-event systems*. Boston, MA: Kluwer Academic Publishers.
- Narendra, K. S., & Thathachar, M. A. L. (1989). *Learning automata: An introduction*. Englewood Cliffs, NJ: Prentice-Hall.
- Patankar, R., Ray, A., & Lakhtakia, A. (1998). A state-space model of fatigue crack dynamics. *International Journal of Fracture*, 90(3), 235–249.
- Passino, K. M., Michel, A. N., & Antsaklis, P. J. (1994). Lyapunov stability of a class of discrete event system. *IEEE Transactions on Automatic Control*, 39(2), 269–279.
- Ramadge, P. J., & Wonham, W. M. (1987). Supervisory control of a class of discrete-event processes. *SIAM Journal of Control and Optimization*, 25(1), 206–230.
- Ray, A., Wu, M.-K., Carpino, M., & Lorenzo, C. F. (1994). Damage-mitigating control of mechanical systems: Parts I and II. *ASME*

*Journal of Dynamic Systems, Measurement and Control*, 116(3), 437–455.

- Ray, A., & Weng, C-K. (1995). Integrated prognostics, maintenance and life extending control of power plants, *Proceedings of instrumentation Control, and automation in the power industry*, Vol. 38 (pp. 67–75).
- Ray, A. (1999). Stochastic modeling of fatigue crack damage for risk analysis and remaining life prediction. *ASME Journal of Dynamic Systems, Measurement and Control*, 121(3) (to appear).
- Ray, A., & Patankar, R. (1999). A stochastic model of fatigue crack propagation under variable-amplitude loading. *Engineering Fracture Mechanics*, 62(4–5), 477–493.
- Rozak, J. N., & Ray, A. (1997). Robust multivariable control of rotorcraft in forward flight. *Journal of the American Helicopter Society*, 42(2), 149–160.
- Rozak, J. N., & Ray, A. (1998). Robust multivariable control of rotorcraft in forward flight: Impact of bandwidth on fatigue life. *Journal of the American Helicopter Society*, 43(3), 195–201.
- Sanghavi, H. A., & Garg, V. K. (1991). *User manual for the finite state machine software library*. EECS Department Report, University of Texas at Austin.
- Stiver, J. A., Antsaklis, P. J., & Lemmon, M. D. (1995). A logical DES approach to the design of hybrid control systems. *Mathematical and Computer Modeling Mathematical and Computer Modeling, Special Issue on Discrete Event Systems*, 23, 55–76.
- Suresh, S. (1991). *Fatigue of materials*. Cambridge, UK: Cambridge University Press.
- Virkler, D. A., Hillberry, B. M., & Goel, P. K. (1979). The statistical nature of fatigue crack propagation. *ASME Journal Engineering Materials and Technology*, 101(2), 148–153.
- Zhang, H., & Ray, A. (1999). Robust damage damage-mitigating control of mechanical structures: Experimental verification on a test apparatus. *ASME Journal of Dynamic Systems, Measurement and Control*, 121(3) (to appear).
- Zhou, K., Doyle, J. C., & Glover, K. (1996). *Robust and optimal control*. Upper Saddle River, NJ: Prentice-Hall.



**Hui Zhang** was born in Jiangsu, China on April 26, 1970. He received the Ph.D. degree in Mechanical Engineering from the Pennsylvania State University in 1999 and both his bachelor and master degrees from the Department of Precision Instruments and Mechanology, Tsinghua University, in 1993 and 1995, respectively. He has been a graduate Research Assistant from 1995 to 1999. Dr. Zhang's research interests are diversified, covering the fields of linear robust control, discrete-event control, and

hybrid systems. Beyond the interest in systems and controls, Dr. Zhang is also involved in instrumentation, opto-mechanical structure design, testing and control. Dr. Zhang is a member of American Society of Mechanical Engineers.



**Asok Ray** received his Ph.D. degree in Mechanical Engineering from Northeastern University, Boston, MA in 1976, and also graduate degrees in each discipline of Electrical Engineering, Mathematics, and Computer Science. Dr. Ray joined the Pennsylvania State University in July 1985, and is currently a Professor of Mechanical Engineering. Prior to joining Penn State, Dr. Ray held research and academic positions at Massachusetts Institute of Technology and Carnegie-Mellon University

as well as research and management positions at GTE Strategic Systems Division, Charles Stark Draper Laboratory, and MITRE Corporation. Dr. Ray has been also a Senior Research Fellow at NASA Lewis Research Center under a National Academy of Sciences award. Dr. Ray's research experience and interests include: Fault-accommodating and robust control systems, Modeling and analysis of thermomechanical fatigue and creep in both deterministic and stochastic settings, Intelligent instrumentation for real-time distributed processes, and Control and optimization of continuously varying and discrete-event dynamic systems, as applied to Aeronautics and Astronautics, Undersea Vehicles and Surface Ships, Power and Processing plants, and Autonomous Manufacturing. Dr. Ray has authored or co-authored 300 research publications including over 130 scholarly articles in refereed journals and research monographs. Dr. Ray is a Fellow of ASME, an Associate Fellow of AIAA, and a Senior Member of IEEE.



**Shashi Phoha** received her Ph.D. degree in Mathematical Statistics from Michigan State University, East Lansing, MI in 1976 and the M.S. degree in Operations Research from Cornell University, Ithaca, NY in 1973. Dr. Phoha is the Head of the Information Science Division and Assistant Director of the Applied Research Laboratory and a Professor of Electrical and Computer Engineering at Penn State University. Her research focuses on information sciences, which bring together

ideas from logic, operations research, formal languages, automata theory, dynamic systems, and control theory in diverse applications. She has diverse experience in multi-organizational collaborative research and in scientific analysis of distributed information. Drawing on her broad scientific background and multidisciplinary research collaborations, she has made outstanding contributions to the scientific analysis of distributed information for decision support, multi-stage coordination and intelligent control of interacting processes in complex dynamic systems. Some of her recent innovations are implemented in the National Information Infrastructure Test bed which is a university/industry partnership, funded by DARPA, for developing web-based mechanisms for sensor and model based health monitoring and failure prognosis in operating machinery. She has established other innovative research directions for understanding ocean and environmental physics through analysis of correlated time-series data collected by a self-reconfiguring network of undersea robotic vehicles.